Noname manuscript No.
(will be inserted by the editor)

Modelling immune memory development

Eleonora Pascucci · Andrea Pugliese

Abstract The cellular adaptive immune response to influenza has been analysed through several recent mathematical models. In particular, Zarnitsyna et al. (2016) show how central memory CD8+ T cells reach a plateau after repeated infections, and analyse their role in the immune response to further challenges. In this paper we further investigate the theoretical features of that model by extracting from the infection dynamics a discrete map that describes the build-up of memory cells. Furthermore, we show how the model by Zarnitsyna et al. (2016) can be viewed as a fast-scale approximation of a model allowing for recruitment of target epithelial cells. Finally, we analyse which components of the model are essential to understand the progressive build-up of immune memory. This is performed through the analysis of simplified versions of the model that include some components only of immune response. The analysis performed may also provide a theoretical framework for understanding the conditions under which two-dose vaccination strategies can be helpful.

Keywords viral-immune mathematical model · secondary infections · immune memory · multiscale model

1 Introduction

Influenza is a serious infectious disease which affects the respiratory tract caused by RNA viruses of the family *Orthomyxoviridae*, the influenza viruses.

E. Pascucci
Dipartimento di Matematica, Università degli Studi di Trento, via Sommarive 14, 38123 Povo (TN), Italy
E-mail: eleonorapascucci11@gmail.com

A. Pugliese
Dipartimento di Matematica, Università degli Studi di Trento, via Sommarive 14, 38123 Povo (TN), Italy
E-mail: andrea.pugliese@unitn.it

Due to its easy spread, every year many people get sick or die, making flu a constant social problem for worldwide public health. Several recent papers present mathematical models for describing immune response to influenza infections.

Many studies have focused on the role of some immune components in the timing and the strength of the infection (Dobrovolny et al., 2013; Iwasaki and Nozima, 1977; Moore et al., 2019; Wu et al., 2018). Li et al. (2021) infer the relationship between the level of macrophage activation and the level of viral shedding. However, a deficiency of several of these studies is that the authors have considered only the case of a single primary infection.

Several papers have however studied the response to repeated infections, whether to homologous or heterologous strains. In particular, McCaw and coworkers have studied in a series of papers (Cao et al., 2016, 2015; Yan et al., 2016, 2019) how viral hierarchy and the interval between infections determine their outcome.

When a short time interval separates exposures, a primary infection protects against a subsequent infection and the target cells present a lower susceptibility to infection with other influenza viruses (Cao et al., 2015). Increasing the time period between two subsequent infections weakens the effectiveness of CD8+ T cells. This, in turn, increases the duration of a second infection and the achieved virus peak value (Zarnitsyna et al., 2016). Innate, humoral adaptive and cellular adaptive immune responses work together to control the infection, but epidemiological studies highlight the inability to quantify which of them is more dominant (Dobrovolny et al., 2013; Yan et al., 2019).

The model by Zarnitsyna et al. (2016) centres on cellular response in the case of a heterologous challenge . A key feature of their model is the distinction between T-cells in lymph nodes and in the respiratory tract. Their results provide a theoretical basis for the build-up of immune response with repeated infections; in fact, it is shown that only after the second infection event, the immune memory reaches a level at which it is able to effectively suppress further infection challenges.

In this note, we intend to further investigate the theoretical features of the model by Zarnitsyna et al. (2016), and to assess which components of the model allow for the progressive build-up of immune memory. A better understanding of different stages and components of the immune response may favour quicker effective treatments against viral infections and the development of vaccines.

First (Section 2), following the informal arguments presented by Zarnitsyna et al. (2016), we build a discrete map that synthetizes any infection event as an input-output map. The shape of the map determines whether a single infection, or several infections, are needed to build-up an effective immune memory.

We continue (Section 3) developing an extended model by allowing for recruitment of new target epithelial cells and several other transitions; the model by Zarnitsyna et al. (2016) can be viewed as a fast-scale approximation of the extended model. In this way, the dynamics of the compartment is modelled also in the intervals between infections, thus allowing for a more thor-

ough exploration of the effect of the length of the interval between consecutive infections on the infection dynamics for different parameter values.

Finally (Section 4), in order to understand which features of the model by Zarnitsyna et al. (2016) allow for a gradual increase of immune memory, we formulate very simplified versions of the model that include some components of immune response only, and study in which cases the immune response increases with every new infection, and when the opposite occurs. Indeed, in several simple models (Diekmann et al., 2018; Nowak and May, 2000) the lower the immune level is (at least, in a certain range of levels) before an infection, the higher it will be afterwards.

While the model by Zarnitsyna et al. (2016) is already a big simplification of the underlying biology, it is way too detailed to be incorporated into a multiscale immuno-epidemiological model (Barbarossa and Röst, 2015; Diekmann et al., 2018; Gandolfi et al., 2015; Gilchrist and Sasaki, 2002); it may then be useful to have a simple model, whose qualitative features resemble those of more realistic models.

2 The model by Zarnitsyna et al. (2016)

The model by Zarnitsyna et al. (2016) was developed for influenza and includes target cells (that may be in susceptible S, infected I or refractory R states), free virus V, antigens A, innate immune response M (a large compartment including natural killer cells, and molecules such as cytokines and interferons) and T-cells in different states (precursor T_P, proliferating T_E, resident T_R and central memory T_M), with the transitions outlined in Fig. 1. One of its main aspects is the focus on the relationship between spatial heterogeneity, T cell differentiation and migration. The authors distinguish proliferating T cells in secondary lymphoid organs, such as lymph nodes, where the expansion of influenza-specific CD8+ T cells occurs, from T cells resident in the respiratory tract, the actual site of infection, where they can kill infected target cells.

The model and its variables are graphically presented in Fig. 1, while the parameter values are in Table 1. Referring to the original paper (Zarnitsyna et al., 2016) for a detailed presentation of the model assumptions, the main transitions are the following:

- Susceptible target cells are infected by free virions, and can also convert into a refractory state R (in which they cannot be infected) under the stimulus of the innate immune components, such as type 1 interferons.
  Recruitment or death of target cells, and reversion from refractory to susceptible state are neglected, since the model is tailored for acute infections, and on that time scale the recruitment and reversion have a limited effect (Zarnitsyna et al., 2016); see Section 3 for relaxing this assumption.
- Infected target cells die at rate δ and release free virions (possibly at cell rupture) at rate p. Infected cells are also killed by T- cells migrated into the respiratory tract. Free virions die at rate c.

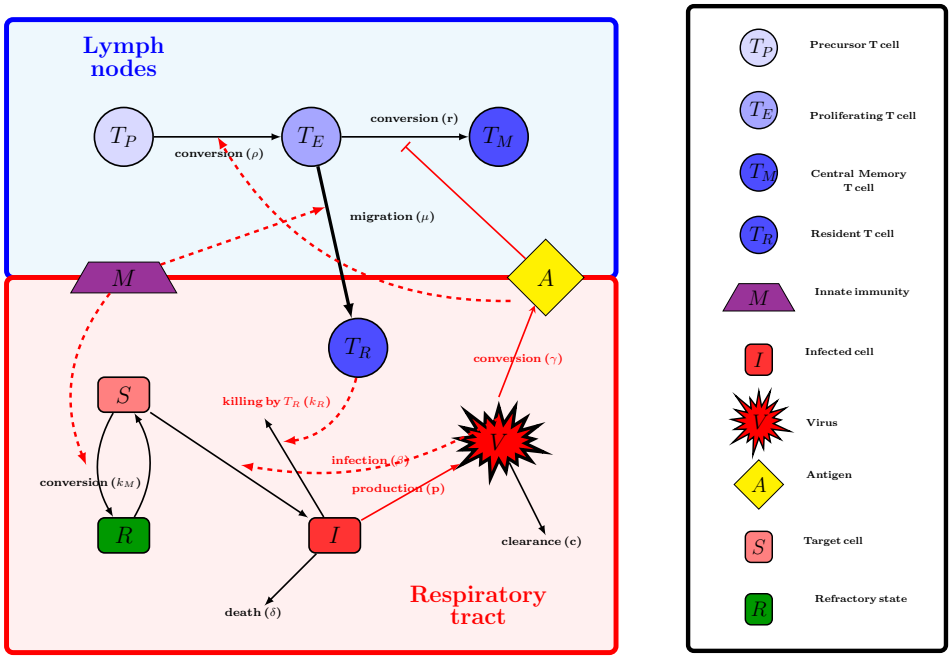

Figure 1 Scheme and variables of the model from Zarnitsyna et al. (2016)

- The innate immune response increases towards its maximal value (set to 1), stimulated (according to a saturated function) by the presence of infected cells, while decreases to 0 in their absence.
- Precursor T cells are recruited into proliferating cells, and these replicate, at rate proportional to $A/(\phi+A)$ where A is the antigen level, and ϕ is the half-saturation constant. At low antigen levels, profilerating T cells either die by apoptosis or differentiate into memory cells. Proliferating T cells in lymphoid organs migrate to the respiratory tract proportionally to the level of local immune response.

The corresponding equations are the following

$$\begin{cases} S'(t) &= -\beta S(t)V(t) - k_M M(t)S(t) \\ I'(t) &= \beta S(t)V(t) - \delta I(t) - k_R T_R(t) I(t) \\ V'(t) &= pI(t) - cV(t) \\ A'(t) &= \gamma V(t) - d_A A(t) \\ M'(t) &= \frac{\sigma_M I(t)}{\phi_M + I(t)}(1 - M(t)) - d_M M(t) \\ T'_P(t) &= -\rho T_P(t) \frac{A(t)}{\phi + A(t)} \\ T'_E(t) &= \rho(T_P(t) + T_E(t)) \frac{A(t)}{\phi + A(t)} \\ &\quad -(\alpha + r) T_E(t) \left(1 - \frac{A(t)}{\phi + A(t)}\right) - \mu T_E(t) M(t) \\ T'_R(t) &= \mu T_E(t) M(t) - d_R T_R(t) \\ T'_M(t) &= r T_E(t) \left(1 - \frac{A(t)}{\phi + A(t)}\right) \\ R'(t) &= k_M M(t) S(t). \end{cases} \tag{1}$$

Table 1 Parameter definitions and default values (time units are d=days). All default values from Zarnitsyna et al. (2016), except for δ_M and V_m which have been chosen by us as reasonable values.

β	virion infection rate	$\text{TCID}_{50}(\text{ml})^{-1}\text{d}^{-1}$	$3 \cdot 10^{-5}$
k_M	rate of conversion to refractory state	$(\text{Cells})^{-1}\ \text{d}^{-1}$	4
δ	death rate of infected cells	d^{-1}	1
k_R	killing rate by resident T-cells	$(\text{Cells})^{-1}\ \text{d}^{-1}$	$7 \cdot 10^{-3}$
p	virion release rate	$\text{TCID}_{50}\text{d}^{-1}$	0.04
c	virion death rate	d^{-1}	3
γ	antigen production	d^{-1}	0.3
d_A	antigen decay rate	d^{-1}	1.7
σ_M	innate immunity growth rate	d^{-1}	1
ϕ_M	half saturation constant for innate immunity	Cells	1
d_M	decay rate of innate immunity	d^{-1}	0.2
ρ	proliferation rate of T-cells	d^{-1}	2.15
ϕ	half saturation constant for adaptive immunity	$\text{TCID}_{50}(\text{ ml})^{-1}$	50
α	death rate of proliferating T-cells	d^{-1}	0.4
r	conversion rate into memory cells	d^{-1}	0.07
μ	migration rate into respiratory tissues	d^{-1}	1.2
d_R	death rate of resident T-cells	d^{-1}	0.1
T_0	initial and equilibrium value of target cells	Cells	$4 \cdot 10^8$
ε	growth rate of target cells (model (7))	d^{-1}	variable
η	reversion from refractory state (model (7))	d^{-1}	variable
δ_M	decay rate of memory cells (model (7))	d^{-1}	10^{-4}
V_m	quantity in the infection rate of target cells (model (7))	$\text{TCID}_{50}(\text{ ml})^{-1}$	10^{-4}

Since it is assumed that there is no reversion back from the refractory state, the equation for $R(t)$ can be omitted.. (Zarnitsyna et al., 2016)3 It can also be seen that the memory cells T_M do not appear to play any role in the model, as the right hand side of (1) does not depend on $T_M(t)$. However they play

a role in secondary infections, as Zarnitsyna et al. (2016) assume that they can play the same role as precursor cells T_P; namely, the initial value of T_P in subsequent infections is taken as the final value of T_M (or of $T_M + T_P$) in previous infections, as their decay rate can be neglected.

These considerations allow us to describe the system analysed by Zarnitsyna et al. (2016) through a discrete map. Precisely, note that all points of the subspace

$$\mathcal{M} = \{(S, T_P, T_M, I, V, A, M, T_E, T_R) \in \mathbb{R}^9_+ : \ I = V = A = M = T_E = T_R = 0\}$$

are equilibria for system (1). Moreover, their stability can be recognized through the quantity

$$R_0 = \frac{\beta S p}{c\delta}. \tag{2}$$

R_0 represents the average value of free virions produced throughout its life by infecting susceptible cells which, in turn, will release free virions. Indeed $\beta S/c$ represents the average number of cells infected by one viral unit, and p/c the average number of viral units released by an infected cell.

The stability of an equilibrium of (1) can be gathered by its Jacobian J that has the structure

$$J = \begin{pmatrix} 0_{1\times 1} & B_{12} & B_{13} \\ 0_{2\times 1} & B_{22} & 0_{2\times 7} \\ 0_{7\times 1} & B_{32} & B_{33} \end{pmatrix} \text{ with } B_{22} = \begin{pmatrix} -\delta & \beta S \\ p & -c \end{pmatrix}.$$

Here $0_{m\times n}$ represents an $m \times n$ matrix, with all entries equal to 0, while the other submatrices have appropriate dimensions.
Because J has recurring block triangular structure, its eigenvalues are 0, the eigenvalues of B_{22} and those of B_{33}. B_{33} is a triangular matrix, whose eigenvalues are its diagonal elements which are either 0 or negative. Both eigenvalues of B_{22} have negative real part if its determinant is positive, i.e. $c\delta > \beta S p$, i.e. $R_0 < 1$. On the other hand, if $R_0 > 1$, one eigenvalue of B_{22} is positive. Hence, if S is such that $R_0 > 1$, i.e. $S > \dfrac{c\delta}{\beta p}$, then the equilibrium is unstable; if it is smaller, by looking at its centre manifold, it can be shown that the equilibrium is attracting from the interior of $\mathbb{R}^9_+$. Leaving out the coordinates equal to 0, we can identify $\mathcal{M}$ with $\mathbb{R}^3_+$, divide it into the repelling and the attracting parts,

$$\mathcal{M}_+ = \{(S, T_P, T_M) \in \mathbb{R}^3_+ : \ S > \frac{c\delta}{\beta p}, \ T_P > 0\}$$

$$\mathcal{M}_- = \{(S, T_P, T_M) \in \mathbb{R}^3_+ : \ S < \frac{c\delta}{\beta p}\}.$$

The solutions of (1) join a starting point P_0 in $\mathcal{M}_+$ to a point P_1 in $\mathcal{M}_-$, thus defining a map from $\mathcal{M}_+$ to $\mathcal{M}_-$.

In order to reduce the problem to a simpler one-dimensional map, we fix $S(0) = T_0$, a level corresponding to a normal healthy individual, and $V(0) = V_0$, the typical level of a virus inoculum, and define a map $F : \mathbb{R}^+ \to \mathbb{R}^+$ as

$$F(T_P) = \lim_{t\to\infty} (T_P(t) + T_M(t))) \tag{3}$$

where $T_P(t)$ and $T_M(t)$ are the corresponding variables in the solution of (1) with

$$T_P(0) = T_P,\ S(0) = T_0,\ V(0) = V_0$$

and all other variables equal to 0 at $t = 0$. The rationale for this choice is that, as stated above, memory cells at the end of an infection episode are taken as equivalent to precursor cells at the beginning of the following one.

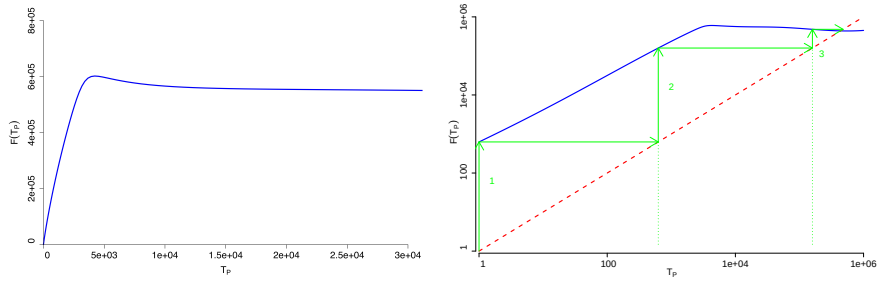

Figure 2 Plot of the function F: a) over the range $[0, 3 \cdot 10^4]$; b) over a larger range in logarithmic scale; the dotted line is the bisectrix $y = T_P$; the arrows indicate the growth of memory cells in a primary (1), secondary (2) or tertiary (3) infection. Parameter values in Table 1.

It seems difficult to establish analytically the properties of the function F. Instead, we computed numerically the function F, adopting the parameter values used in Zarnitsyna et al. (2016), for all realistic values of $T_{P,0}$; all computations have been performed using the `ode15s` function of Matlab with `RelTol`$= 10^{-8}$ and `AbsTol`$= 10^{-10}$, after having scaled all variables (except for $M(t)$) by dividing them by T_0. The Matlab code used for this will be made available on-line.

It has been found that $F(T_{P,0})$ reaches a maximum, and then starts to decrease (Fig. 2a); extending the range of $T_{P,0}$, one sees that for higher values of $T_{P,0}$ $F(T_{P,0})$ is again increasing, apparently to infinity (Fig. 2b). However, by overlaying the bisectrix $y = T_P$ (dotted line in Fig. 2b), one sees that, for any value of $T_{P,0}$ around 1, after two iterations $F^n(T_{P,0})$ will be between 10^5 and 10^6 and will quickly converge to the point T^* where the function F and the bisectrix cross.

In other words, for the parameter values used and for the values of $T_{P,0}$ which are reasonable for a naive individual (Zarnitsyna et al., 2016) $T_{P,0} \ll F(T_{P,0}) \ll F^2(T_{P,0})$ while $F^2(T_{P,0}) \approx F^3(T_{P,0}) \approx \cdots \approx F^n(T_{P,0}) \approx T^*$. In

this notation $F^n(T_{P,0})$ represents the initial value of precursor T-cells of an individual that has already been infected n times with the virus.

The left panel of Fig. 3 shows how the infection pattern along the solutions of (1) strongly depends on the initial value $T_P(0)$, confirming what is shown by Zarnitsyna et al. (2016): if initially $T_{P,0}$ is close to the value of T_M at the end of a primary infection, the peak value of I and V (dashed lines in Fig. 3) are close to those obtained in case of a primary infection (solid lines), but the infection length is much shorter; if the initial value of T_P is close to the value of T_M at the end of this secondary infection (dotted lines), the peak infection values decrease by a couple of orders of magnitude, presumably resulting in negligible health effects.

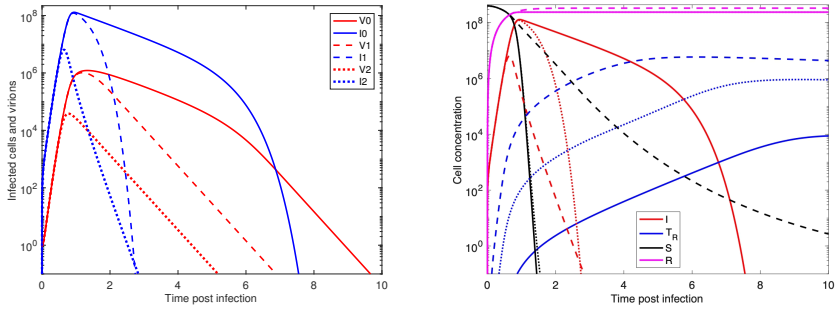

Figure 3 Left panel: $I(t)$ and $V(t)$ solutions of (1) for different values of $T_P(0)$: $I0$ and $V0$ correspond to $T_P(0) = 1$; $I1$ and $V1$ to $T_P(0) = 6.26 \cdot 10^2 = T_{P,0}(\infty) + T_{M,0}(\infty)$; $I2$ and $V2$ to $T_P(0) = 1.59 \cdot 10^5 = T_{P,1}(\infty) + T_{M,1}(\infty)$. Right panel: Variables $I(t)$, $T_R(t)$, $S(t)$ and $R(t)$ in the same solutions of (1) as in left panel; solid lines correspond to $I0$ and $V0$, dotted lines to $I1$ and $V1$, dashed lines to $I2$ and $V2$. Other initial values and parameters in Table 1.

To better understand the mechanism behind these differences, it is helpful to observe other variables of the system (right panel of Fig. 3). First of all, note that $I_0(t)$ has three different exponential phases: in the first period, its growth rate is close to

$$r = \sqrt{p\beta T_0 + \frac{(c-\delta)^2}{4}} - \frac{(c+\delta)}{2}, \tag{4}$$

since $S(t)$ is close to the initial value T_0. At the end of this period, $S(t)$ drops around 0, since, under the action of the innate immune response, most target cells convert to the refractory state; hence, $I_0(t)$ decays at rate δ, as the resident T cells are still at low concentrations. When $T_R(t)$ reaches values around 10^2, the factor $k_R T_R(t)$ is no longer negligible and the decay of $I_0(t)$ occurs approximately at a rate $\delta + k_R\overline{T_R}$ where $\overline{T_R}$ represents an average value of $T_R(t)$ in this final phase.

In a secondary infection, because of the recruitment of memory cells, $T_R(t)$ reaches values of the order 10^2 at the same time as $S(t)$ starts dropping from

the initial value T_0; thus, there are only two phases in the dynamics of infected cells $I(t)$, the second one being a decay with approximate rate $\delta + k_R\overline{T_R}$ where $\overline{T_R}$ is again the average value of $T_R(t)$ in the second phase, which is higher than in the case of a primary infection.

Finally, in a tertiary infection, $T_R(t)$ reaches values of the order 10^2 before any significant decrease of $S(t)$; this means that the phase of exponential growth of $I(t)$ is shorter and the peak value lower than in the previous cases; correspondingly $S(t)$ decreases much more slowly, and this in turn causes a slightly lower rate of decrease of $I(t)$. Although $T_E(t)$ is initially larger, like $T_R(t)$, than in secondary infection, the lower values reached by $A(t)$ make it increase less after the peak, so that the final value of $T_M(t)$ are comparable, as shown by Fig. 2b.

Clearly, these specific results are contingent upon the parameter values estimated by Zarnitsyna et al. (2016). One of the most relevant ones is the replication rate ρ of proliferating T cells; if it were increased by 50%, one infection would suffice to develop enough immune memory to control all further infectios; if it were decreased by 50%, the adaptive immune system would not be effective at all, and the control of infections would be due to the innate system only (simulations not shown).

3 A multiscale model

3.1 Formulation and short-term dynamics

In the previous Section, it was implicitly assumed that between one infection and the next one the target cells had recovered their initial level, through the production of new cells and the reversion from refractory to sensitive state, that all proliferating and effector T-cells had disappeared, while memory T cells were at the level achieved after last infection.

In order to discuss how the length τ of the interval between infection affected the dynamics, Zarnitsyna et al. (2016) assumed that in a secondary infection proliferating and effector T-cell started from the level $T_E(\tau)$ and $T_R(\tau)$ reached in the primary infection, while susceptble target cells were anyway at the initial level T_0. In this way, Zarnitsyna et al. (2016) show how an infection after $\tau = 30$ days is completely controlled by resident T cells, while one after $\tau = 1$ year is described by the simulations shown in Fig. 3. However, the assumption appears somewhat artificial, and it makes it impossible to assess for which rates of recruitment and reversion to susceptibility of target cells the picture is correct: if the recruitment of target cells is very slow, they might not have returned to the original level in 30 days, while if it is large, the dynamics provided by (1) may be inaccurate, since this process is neglected there.

In order to address these questions, we present here a model where all these transitions are incorporated into the differential equations, allowing for

a continuous description of the dynamics with and without infection. We start from model (1), adding the necessary transitions.

First, we assume that target cells in the refractory state, R, will revert to sensitive state at rate η (a small parameter). We also assume that target cells (both in sensitive and refractory state) will proliferate according to a logistic model (an assumption used in several models e.g., Cao et al. (2015); Yan et al. (2019)) at rate $\varepsilon\left(1-\frac{T+R+I}{T_0}\right)$, where T_0 represents the healthy values (to which they would return after perturbations) for target cells, where ε is another small parameter.

Furthemore, we assume that also memory cells will die but over a very long time scale, much longer than the scale over which target cells recover their normal density; we assume a rate $\delta_M \ll \varepsilon$.

These assumptions translate into the following model

$$\begin{cases} S'(t) &= -\beta S(t)V(t) - k_M M(t)S(t) + \eta R(t) \\ & \quad +\varepsilon(S(t)+R(t))\left(1-\frac{S(t)+R(t)+I(t)}{T_0}\right) \\ R'(t) &= k_M M(t)S(t) - \eta R(t) \\ I'(t) &= \beta S(t)V(t) - \delta I(t) - k_R T_R(t) I(t) \\ V'(t) &= pI(t) - cV(t) \\ A'(t) &= \gamma V(t) - d_A A(t) \\ M'(t) &= \frac{\sigma_M I(t)}{\phi_M + I(t)}(1-M(t)) - d_M M(t) \\ T_P'(t) &= -\rho T_P(t)\frac{A(t)}{\phi+A(t)} \\ T_E'(t) &= \rho(T_P(t)+T_E(t))\frac{A(t)}{\phi+A(t)} \\ & \quad -(\alpha+r)T_E(t)\left(1-\frac{A(t)}{\phi+A(t)}\right) - \mu T_E(t)M(t) \\ T_R'(t) &= \mu T_E(t)M(t) - d_R T_R(t) \\ T_M'(t) &= rT_E(t)\left(1-\frac{A(t)}{\phi+A(t)}\right) - \delta_M T_M(t). \end{cases} \tag{5}$$

If we set $\varepsilon = \eta = \delta_M = 0$, (5) reduces to (1) that can then be considered as an approximation over short time scales.

However, system (5) cannot effectively represent the long-term dynamics over repeated infections.

One problem is that memory cells do not affect the dynamics of the system, as the equations of the other variables are independent of T_M. To obviate this problem, we choose a simple modification of the system, in the spirit of the assumption by Zarnitsyna et al. (2016) that memory cells are equivalent to precursor cells in subsequent infections. For the sake of simplicity, we assume that memory cells can differentiate exactly as precursor cells at all times. Namely, we modify the equations for T_E' and T_M' in (5) to

$$\begin{aligned} T_E'(t) &= \rho(T_P(t)+T_E(t)+T_M(t))\frac{A(t)}{\phi+A(t)} \\ & \quad -(\alpha+r)T_E(t)\left(1-\frac{A(t)}{\phi+A(t)}\right) - \mu T_E(t)M(t) \\ T_M'(t) &= rT_E(t)\left(1-\frac{A(t)}{\phi+A(t)}\right) - \rho T_M(t)\frac{A(t)}{\phi+A(t)} - \delta_M T_M(t). \end{aligned} \tag{6}$$

To understand the other problem, note that for system (5)–(6) the subspace of infection-free equilibria is

$$\{(T_0, T_P, 0, 0, 0, 0, 0, 0, 0, 0)\}$$

where only the coordinate T_P is arbitrary.

Such equilibria are unstable if and only if $R_0 > 1$, independently of the value of T_P.
If $R_0 < 1$, infections are impossible. If $R_0 > 1$ (as it will always be assumed), solutions of (5), starting close to the equilibrium with $V(0) = V_0$, will follow the path of Fig. 3 with a large increase of $V(t)$ and $I(t)$ followed by a quick decrease towards 0. However, as the solutions approach again the infection-free equilibrium, $I(t)$ and $V(t)$ start increasing again, as soon as $R_0 \frac{S(t)}{T_0} > 1$, giving rise to a second infection episode, in absence of any reinfection, and possibly arriving, after several infection cycles, to a chronically infected state (see Hancioglu et al., 2007). We deem that for many infections (e.g. influenza, for which parameter values have been set) such dynamics is non-realistic. When the model predicts extremely low values for $I(t)$ or $V(t)$, that state should be interpreted as a virus-free host, and thus a new infection episode should require a reinfection.

A possible solution is to set up a stochastic model, in which numbers of cells can only have integer values. A simpler solution is to modify the rule for infections of target cells in (5), making the equilibria stable. Precisely, the term $\beta S(t)V(t)$ is multiplied by the factor $V/(V + V_m)$ where V_m is a very small value (we choose $V_m = 10^{-4}$, but the exact value is largely irrelevant); in this way, the dynamics is basically identical to (5) as long as $V \gg V_m$, but the infection-free equilibria become stable (the model becomes a so-called excitable system). Through this term, we are assuming that a very small virus inoculum is insufficient to cause an infection, although the actual mechanisms may be different (Li and Handel, 2014; Pugliese and Gandolfi, 2008).

Hence, the final system that we consider is

$$\begin{cases} S'(t) &= -\beta S(t)\frac{V^2(t)}{V_m+V(t)} - k_M M(t)S(t) + \eta R(t) \\ &\quad +\varepsilon(S(t)+R(t))\left(1-\frac{S(t)+R(t)+I(t)}{T_0}\right) \\ R'(t) &= k_M M(t)S(t) - \eta R(t) \\ I'(t) &= \beta S(t)\frac{V^2(t)}{V_m+V(t)} - \delta I(t) - k_R T_R(t) I(t) \\ V'(t) &= pI(t) - cV(t) \\ A'(t) &= \gamma V(t) - d_A A(t) \\ M'(t) &= \frac{\sigma_M I(t)}{\phi_M+I(t)}(1-M(t)) - d_M M(t) \\ T_P'(t) &= -\rho T_P(t)\frac{A(t)}{\phi+A(t)} \\ T_E'(t) &= \rho(T_P(t)+T_E(t)+T_M(t))\frac{A(t)}{\phi+A(t)} \\ &\quad -(\alpha+r)T_E(t)\left(1-\frac{A(t)}{\phi+A(t)}\right) - \mu T_E(t)M(t) \\ T_R'(t) &= \mu T_E(t)M(t) - d_R T_R(t) \\ T_M'(t) &= rT_E(t)\left(1-\frac{A(t)}{\phi+A(t)}\right) - \rho T_M(t)\frac{A(t)}{\phi+A(t)} - \delta_M T_M(t). \end{cases} \tag{7}$$

One may note that, if decay of memory cells is neglected ($\delta_M = 0$), one can introduce a variable $\tilde{T}_P(t) = T_P(t) + T_M(t)$ instead of the two variables $T_P(t)$ and $T_M(t)$, obtaining an equivalent system. We prefer to keep both variables, in order to be able to track the dynamics of memory cells.

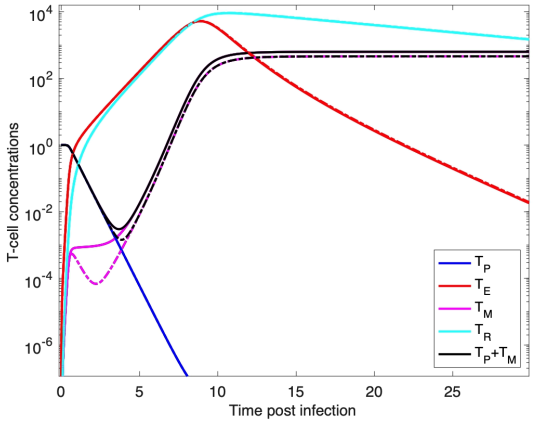

Figure 4 $T_P(t)$, $T_E(t)$, $T_R(t)$ and $T_M(t)$ solutions of (1) (solid lines) and of (7) with $\varepsilon = \eta = \delta_M = 0$ (dashed-dotted lines). The dashed-dotted line is visible only for $T_M(t)$ and the sum $T_P(t) + T_M(t)$, as the values of the other variables are practically identical in the two system. Parameter values in Table 1.

First of all, we wish to show how the dynamics of (7) with $\varepsilon = \eta = \delta_M = 0$ compares to that of (1) (Fig. 4). As can be seen, the main difference being

the behaviour of memory cells that show a transient decrease in the increasing phase of infection. This is a consequence of the modified equations (6) that allow memory cells to form during the early phase of infection (when antigen concentration is low) and then immediately differentiate into proliferating cells, as antigen concentration increases. This phenomenon is probably not realistic, but its quantitative impact is small (consider the logarithmic scale in Fig. 4) and, since the sum $T_P(t) + T_M(t)$ is very similar in the two cases at all times, does not affect significantly the final level of memory cells. Therefore, we avoid complicating the system with other stages and/or delays.

Furthermore, we wish to see how the system is sensitive to the values of η and ε. In Fig. 5, we show some simulations of (7) for different levels of the parameters ε and η (and $\delta_M = 0$), showing convergence to the corresponding simulation with $\varepsilon = \eta = 0$.

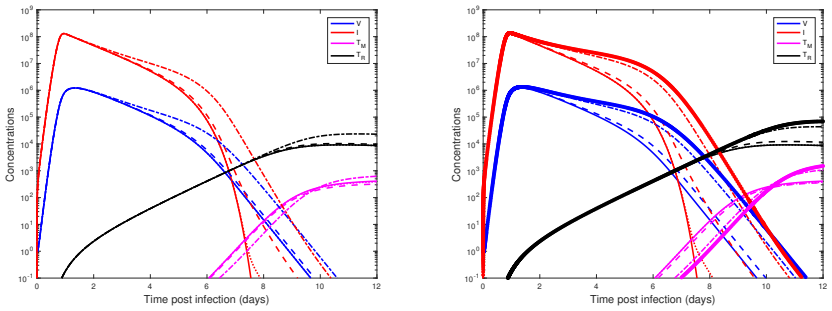

Figure 5 Left panel: simulations for primary infection dynamics of system (7) for different values of ε with $\eta = 0$: $\varepsilon = 0$ (solid lines) , $\varepsilon = 10^{-4}$ (dotted lines), $\varepsilon = 10^{-2}$ (dashed lines), $\varepsilon = 0.1$ (dashed-dotted lines). Right panel: simulations for primary infection dynamics of systems (5) for different values of ε and η: $\varepsilon = \eta = 0$ (solid lines); $\varepsilon = 0$, $\eta = 10^{-4}$ (dotted lines); $\varepsilon = 0$, $\eta = 10^{-2}$ (dashed lines); $\varepsilon = 0$, $\eta = 0.1$ (dashed-dotted lines); $\varepsilon = \eta = 0.1$ (thick lines with symbols). In both panels, lines of different colours correspond to different variables of the system, according to the legend. Other parameter values are in Table 1.

Considering the effect of the parameters ε and η, this is most visible in the dynamics of the infected target cells $I(t)$; even when η or ε are equal to 10^{-4}, there is a noticeable difference (but remember the logarithmic scale) from $\varepsilon = \eta = 0$ in the values of $I(t)$ late in the infection. The differences increase when η or ε are larger and, when either η or ε or both are equal to 0.1, a difference emerges also in the values of $I(t)$ immediately after the infection peak, so that infected cells maintain values above 10^6 for about a day longer than with $\varepsilon = \eta = 0$. Minor differences appear also in the other variables. Still, the overall infection dynamics is very similar with $\eta = \varepsilon = 0$ or $\varepsilon = \eta = 0.1$; the main difference is that a few more days are needed for complete clearance of infected cells.

This comparison appears to justify the use of (1) to analyse the short-term infection dynamics, as in Zarnitsyna et al. (2016). For instance, with the values

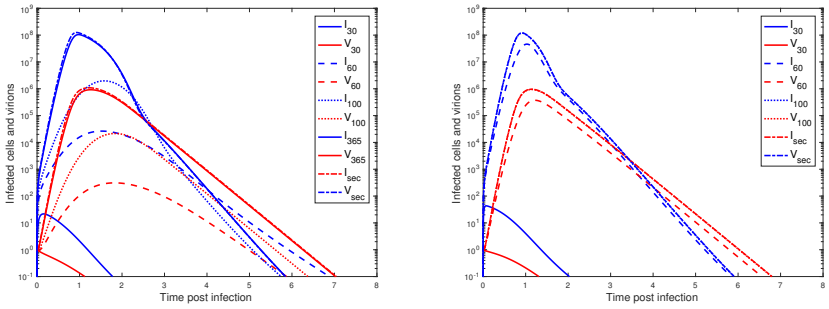

Figure 6 $I(t)$ and $V(t)$ solutions of system (7) starting after a reinfection. I_x and V_x represent a reinfection x days after a first infection. I_{sec} and V_{sec} instead represent solutions of system (7) starting with initial values as for the secondary infections in Fig. 3. Left panel: $\varepsilon = \eta = 0.01$; right panel $\varepsilon = \eta = 0.1$. Other parameter values are in Table 1.

used by Cao et al. (2015) ($\varepsilon = 0.8$, $\eta = 0.05$), the short-term dynamics (not shown) is similar to that with $\varepsilon = \eta = 0.1$, though infected cells maintain high values a bit longer.

3.2 Long-term dynamics and reinfections

It seems natural asking whether reinfections in model (5) induce a similar pattern to what is shown in Fig. 2b. As discussed above, when reinfections are considered in (1), as summarized in the function F, it is assumed that the target cells had recovered their initial level, and that all proliferating and effector T-cells had disappeared. On the other hand, the interval between infections should have a relevant effect on infection outcome, as shown by Cao et al. (2015) and partly in Zarnitsyna et al. (2016).

In Fig. 6 we show, for different values of the parameters ε and η, simulations of the dynamics after a reinfection, i.e. a quantity V_0 is added to $V(t)$ at some time t after the first infection.

It can be seen that, if $t = 30$ (i,e,, a reinfection occurs 1 month after the first infection), the infected target cells are immediately destroyed by the T cells still present at high concentrations in the respiratory tissue (T_R), and no substantial infection occurs, for all values of the parameters η and ε. This confirms the results shown in Zarnitsyna et al. (2016). If the second infection occurs later ($t = 60$ or $t = 100$), the dynamics depends on whether target cells have already recovered the equilibrium value T_0 (right panel: $\varepsilon = \eta = 0.1$) or not yet (left panel: $\varepsilon = \eta = 0.01$); in any case for large delays ($t = 365$), the pattern after the second infection becomes almost identical to that of the second infection seen in Fig. 3.

4 Simplified immune models

4.1 Base simplified model

The simulations of the previous Section show that (1) successfully predicts the short-term dynamics of a primary infection in the more complex model (7); and that the function F built from that (Fig. 2) can be used for predicting the outcome of secondary (or tertiary infections), at least if the intervals between reinfections are long enough.
We plan here to assess which features of the model (1) are responsible for the shape of the function F, connecting the number of precursor T-cells at the beginning of an infection to those present at the beginning of a further infection event. In order to do so, we analysed simplified versions of (1) that included or not some features. The resulting models are not expected to be quantitatively realistic, but their qualitative agreement with Figures 2 and 3 is examined.

All models considered allow for a single variable, $I(t)$, to represent infected cells, assuming that viral load $V(t)$ and antigen concentration $A(t)$ will be proportional to it. This is not quite true (see for instance Fig. 3), especially because of the difference in decay rates, but seems to be a simplification that does not affect the qualitative behaviour of solutions.
Precisely, assume in (1) $V' = A' = M' = 0$. This yields

$$V = \frac{p}{c} I \qquad A = \frac{\gamma}{d_A} V = \frac{\gamma p}{c d_A} I \qquad M = \frac{\frac{\sigma_M}{\sigma_M + d_M} I}{I + \frac{d_M \phi_M}{\sigma_M + d_M}}. \tag{8}$$

Substituting these relations in (1), neglecting the innate immune response $M(t)$ and the refractory state of target cells leads to the following model

$$\begin{cases} S'(t) &= -\beta' S(t) I(t) - k'_M S(t) \frac{I(t)}{\phi'_M + I(t)} \\ I'(t) &= \beta' S(t) I(t) - k_R T_R(t) I(t) - \delta I(t) \\ T'_P(t) &= -\rho T_P(t) \frac{I(t)}{\phi' + I(t)} \\ T'_E(t) &= \rho (T_P(t) + T_E(t)) \frac{I(t)}{\phi' + I(t)} \\ & \quad -(\alpha + r) T_E(t) \left(1 - \frac{I(t)}{\phi' + I(t)}\right) - \mu' T_E(t) \frac{I(t)}{\phi'_M + I(t)} \\ T'_R(t) &= \mu' T_E(t) \frac{I(t)}{\phi'_M + I(t)} - d_R T_R(t) \\ T'_M(t) &= r T_E(t) \left(1 - \frac{I(t)}{\phi' + I(t)}\right) \end{cases} \tag{9}$$

where

$$\beta' = \frac{p\beta}{c} \quad k'_M = \frac{k_M \sigma_M}{\sigma_M + d_M} \quad \mu' = \frac{\mu \sigma_M}{\sigma_M + d_M} \quad \phi' = \frac{c d_A \phi}{\gamma p} \quad \phi'_M = \frac{d_M \phi_M}{\sigma_M + d_M}. \tag{10}$$

One may notice that the action of innate immunity $M(t)$ on target cells and on the migration of central effector cells to the respiratory tract has been substituted with the saturating function in $I(t)$: $\frac{I(t)}{\phi'_M + I(t)}$.

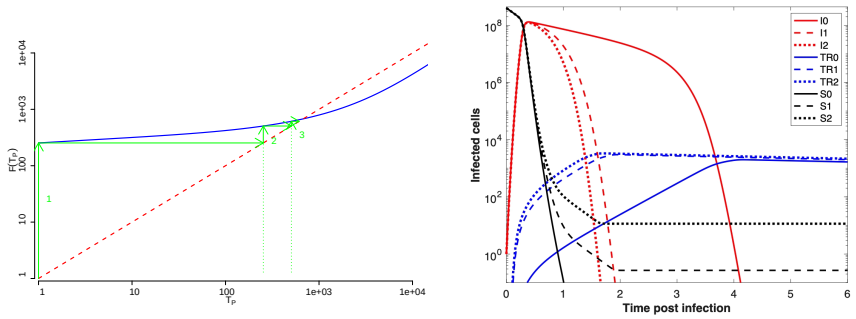

Figure 7 a) Plot of the map F resulting from (9) together with the bisectrix (dashed line); b) the variables $I(t)$, $T_R(t)$ and $S(t)$, solutions of (9) for different values of $T_P(0)$: $I0$ correspond to $T_P(0) = 1$; $I1$ to $T_P(0) = 834 = T_{P,0}(\infty) + T_{M,0}(\infty)$; $I2$ to $T_P(0) = 2023 = T_{P,1}(\infty) + T_{M,1}(\infty)$. Parameter values are $\beta' = 2.5 \cdot 10^{-7}$, $k'_M = 3.33$, $\mu' = 1$, $\phi' = 2.12 \cdot 10^4$, $\phi'_M = 0.8$, $k_R = 0.0125$, $\rho = 3.5$. Other parameter values are as in Table 1.

In the right panel of Fig. 7, the values of $I(t)$ are shown for three simulations of model (9) corresponding to a primary, secondary or tertiary infections. Most parameter values are the same as for (1) from Table 1 with the conversions (10), but β' was chosen a bit lower, and k_R and ρ somewhat larger (see the caption), in order that the peak values of $I(t)$ and $T_R(t)$ were similar to the simulations of Fig. 3. Anyway, the solutions with all the values as in Table 1 (not shown) are qualitatively similar to those of Fig. 7.

The dynamics of the infections in (9) is faster than in (1); this is expected, since the initial growth rate of $I(t)$ in model (1) is r given by (4) while in (9) is $r' = \beta' T_0 - \delta$; a simple computation shows that, if $R_0 > 1$, $r' > r$, and this holds even with the choice of $\beta' < \frac{p\beta}{c}$ used in Fig. 7.

For the rest, the qualitative behaviour of (9) appears similar to that of (1). For instance, the map F built from model (9) is increasing over all its range, and iterates $F^n(T_{P,0})$ quickly converge to a limiting value (Fig. 7a). Conversely, F is not as flat as in the case of (1) around the limiting point; this means that the number of memory cells formed increases with every new infection, and does not plateau after the second infection.

A second difference can be seen by looking at the development over time of infections started with different numbers of precursor cells: in this case, the peak viral load does not decrease when the number of precursor T-cells is high; the only effect is on the infection length (Fig. 7b). This is presumably due to the faster growth rate of infected cells in the first exponential phase; even in tertiary infections, $T_R(t)$ does not reach values of the order of 10^2 before a big drop in susceptible target cells.

One of the properties that (9) shares with (1) is that the higher the level of immune response before an infection is, the more memory cells will be present afterwards. As discussed in the Introduction, many simple models of virus-immune response have instead the opposite feature: the lower the immune

level before an infection is, the higher it will be afterwards. In order to understand which model features favour either property, we considered two further simplifications of (9). In one of them we neglected depletion of target cells; namely, we assumed that whichever is the level of viral infection, target cells are promptly recruited and kept at a fixed density. In the other simplification, we neglected the migration of effector T-cells to the periphery, and assumed that effector T-cells were immediately effective against the infection.

4.2 Model without target cell depletion

The model is like (9), except that $S(t)$ is fixed at the level T_0. Hence

$$\begin{cases} I'(t) &= \beta' T_0 I(t) - k_R T_R(t) I(t) - \delta I(t) \\ T'_P(t) &= -\rho T_P(t) \frac{I(t)}{\phi' + I(t)} \\ T'_E(t) &= \rho (T_P(t) + T_E(t)) \frac{I(t)}{\phi' + I(t)} \\ & \quad -(\alpha + r) T_E(t) \left(1 - \frac{I(t)}{\phi' + I(t)}\right) - \mu' T_E(t) \frac{I(t)}{\phi'_M + I(t)} \\ T'_R(t) &= \mu' T_E(t) \frac{I(t)}{\phi'_M + I(t)} - d_R T_R(t) \\ T'_M(t) &= r T_E(t) \left(1 - \frac{I(t)}{\phi' + I(t)}\right) \end{cases} \tag{11}$$

In this case it can be seen from Fig. 8a) that the function F is decreasing over the relevant range: in other words, the number of memory cells is higher after the primary infection than after further infections.
Correspondingly, the viral level is effectively controlled already in a second infection, slightly better than in a third infection (Fig. 8b). Fig. 8b) shows also that the viral dynamics consists only of two phases: exponential growth until the point the immune system has grown enough to bring it to anexponential decrease. Instead, as already discussed, in models (1) and (9) one can see (Figures 3 and Fig. 7b) three phases in the primary infections where viral exponential growth is first slowed down by target cells depletion, before the immune system sets in to cause fast exponential decrease of virus concentration.

Note that in this simulation we decreased the value of T_0 by one order of magnitude compared to the value used for (1) or (9); otherwise, without depletion of target cells, the viral density would grow to unrealistically high values before being contrasted by the immune system. Equivalently, we could have decreased the attack rate β.

A relevant difference between the previous models (1) or (9) and the current (11) is its long-term behaviour. Indeed, while the former systems have only infection-free equilibria, the latter, since susceptible target cells are constant, has (not considering the compartment T_M) an infected equilibrium $E^* = (I^*, 0, T_E^*, T_R^*)$ under the conditions

$$\beta' T_0 > \delta \text{ and } \rho > 2(\alpha + r) + \mu'.$$

Its coordinates are

$$T_R^* = (\beta' T_0 - \delta)/k_R \qquad T_E^* = d_R T_R^* (\phi'_M + I^*)/(\mu' I^*)$$

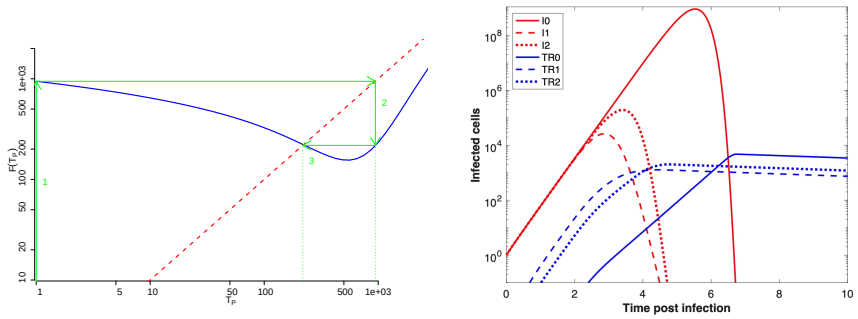

Figure 8 a) Plot of the function F resulting from (11) together with the bisectrix (dashed line); b) the variables $I(t)$ and $T_R(t)$, solutions of (11) for different values of $T_P(0)$: $V0$ correspond to $T_P(0) = 1$; $V1$ to $T_P(0) = 944.3 = T_{P,0}(\infty) + T_{M,0}(\infty)$; $V2$ to $T_P(0) = 216.8 = T_{P,1}(\infty) + T_{M,1}(\infty)$. $T_0 = 2 \cdot 10^7$; other parameter values as in Fig. 7.

while I^* is the only positive solution of

$$I^2(\rho > 2(\alpha+r)+\mu) + I(\phi'_M(\rho - 2(\alpha+r)) - \phi'(\mu+\alpha+r)) - (\alpha+r)\phi'_M\phi' = 0.$$

For the parameter values used in the simulations, this equilibrium is unstable, and the solutions appear to converge to a periodic solution. For other parameter values E^* is asymptotically stable.

Since models (1), (9) and (11) make sense only for short-term dynamics, we are not interested in determining its exact long-term dynamics. However, it can provide an explanation for the shape of the function F in case of (11). We will examine this in the further simplified model (13).

4.3 Model with central effector cells immediately effective

This model is another variant of (9) in which viral cells are killed by the central effector cells, without need for migration to respiratory tracts.

The simplest change is to let infected cells be killed by proliferating T-cells, $T_E(t)$, and, at the same time, ignoring their migration to the respiratory tissues. The resulting equations are

$$\begin{cases} S'(t) &= -\beta' S(t) I(t) - k'_M S(t) \frac{I(t)}{\phi'_M + I(t)} \\ I'(t) &= \beta' S(t) I(t) - k_R T_E(t) I(t) - \delta I(t) \\ T'_P(t) &= -\rho T_P(t) \frac{I(t)}{\phi' + I(t)} \\ T'_E(t) &= \rho (T_P(t) + T_E(t)) \frac{I(t)}{\phi' + I(t)} \\ &\quad -(\alpha + r) T_E(t) \left(1 - \frac{I(t)}{\phi' + I(t)}\right) \\ T'_M(t) &= r T_E(t) \left(1 - \frac{I(t)}{\phi' + I(t)}\right). \end{cases} \tag{12}$$

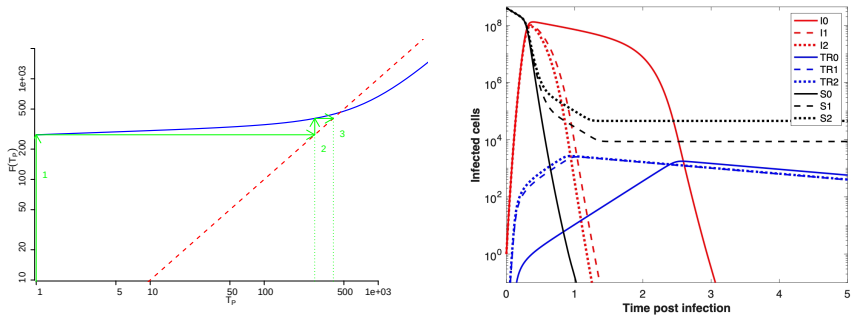

Figure 9 a) Plot of the function F resulting from (12) together with the bisectrix (dashed line); b) The variables $I(t)$, $T_E(t)$ and $S(t)$, solutions of (12) for different values of $T_P(0)$: $I0$ correspond to $T_P(0) = 1$; $I1$ to $T_P(0) = 277.6 = T_{P,0}(\infty) + T_{M,0}(\infty)$; $I2$ to $T_P(0) = 403.9 = T_{P,1}(\infty) + T_{M,1}(\infty)$. Parameter values as in Fig. 7.

In this case, the function F is rather similar to the case of (9) (Fig. 9a), as is the pattern in primary, secondary and tertiary infections (Fig. 9b) , except that the dynamics is even faster.

4.4 Model with central effector cells immediately effective and without target cell depletion

Putting together the simplifcations of (11) and (12), we obtain

$$\begin{cases} I'(t) &= \beta' T_0 I(t) - k_R T_E(t) I(t) - \delta I(t) \\ T'_P(t) &= -\rho T_P(t) \frac{I(t)}{\phi' + I(t)} \\ T'_E(t) &= \rho (T_P(t) + T_E(t)) \frac{I(t)}{\phi' + I(t)} - (\alpha + r) T_E(t) \left(1 - \frac{I(t)}{\phi' + I(t)}\right) \\ T'_M(t) &= r T_E(t) \left(1 - \frac{I(t)}{\phi' + I(t)}\right). \end{cases} \tag{13}$$

The system is too simplistic even to yield a reasonable short-term dynamics in repeated reinfections. However, its analysis can provide a plausible explanation about why in a model without target cell depletion as (11), the higher (at least up to a certain level) the initial level of precursor or memory T cells, the lower their level will be at the end of an infection.

Indeed in (13) (like in the previous short-term ones), memory cells play no role and , in presence of an infection, precursor cells turn into proliferating T cells. Hence, after a short transient period, we can approximate (13) with the 2-dimensional system

$$\begin{cases} I'(t) &= \beta' T_0 I(t) - k_R T_E(t) I(t) - \delta I(t) \\ T'_E(t) &= \rho T_E(t) \frac{I(t)}{\phi' + I(t)} - (\alpha + r) T_E(t) \left(1 - \frac{I(t)}{\phi' + I(t)}\right) \end{cases} \tag{14}$$

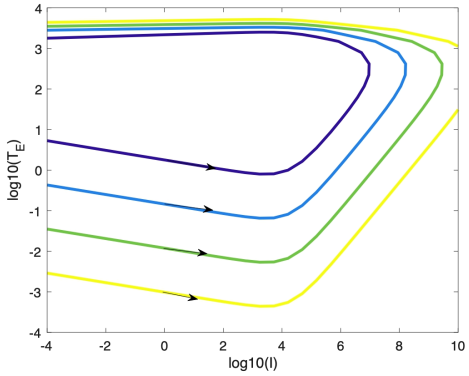

Figure 10 Some solutions of (14) for different initial values. Parameter values as in Fig. 8.

System (14) has the structure of a Lotka-Volterra predator-prey system. If

$$\beta' T_0 > \delta \text{ and } \rho > 2(\alpha + r)$$

there exists an equilibrium

$$E^* = (I^*, T_E^*) \text{ with } I^* = \frac{\phi'(\alpha + r)}{\rho - 2(\alpha + r)},\ T_E^* = \frac{\beta' T_0 - \delta}{k_R}$$

and the quantity

$$U(I, T_E) = \frac{\rho - \alpha - r}{k_R} \log\left(\frac{\phi' + I}{\phi' + I^*}\right) - \frac{a + r}{k_R} \log\left(\frac{I}{I^*}\right) + T_E - T_E^* - T_E^* \log\left(\frac{T_E}{T_E^*}\right)$$

is constant along the solutions of (14).

Some solutions are shown in Fig. 10 from which it appears that solutions starting around the beginning of an infection with a lower value of T_E (resulting from the conversion of a lower initial value of T_P) end up with a higher value of T_E (a part of which will then by recruited as memory cells) at the end of the infection. The solutions of (14) (and presumably of (13)) continue to oscillate periodically, but, as already discussed, the systems in this Section make sense only for a single infection.

5 Conclusions

We have re-analysed the model proposed by Zarnitsyna et al. (2016), clarifying better how its behaviour in subsequent infections relates to the properties of the discrete map F (Fig. 2). In particular, the fact that full immunity is essentially acquired after two infections depends on the fact that F is an increasing function over an interval that includes $(T_{P,0}, F(T_{P,0}))$, where $T_{P,0}$ is the initial level of precursor T-cells, but essentially flat for larger values.

The conclusion seems quite robust, although the exact shape of the function F (and thus the build-up of memory cells) will depend on parameter values, and on details of the model.

We have also shown how that model can be seen as the short time-scale approximation of a multi-scale model (7) that allows for recovery of target cells, and also for loss of memory cells. Whether reinfections can be approximated through the fast equations (1), connected by the discrete map F, depends on the interval occurring between reinfections, in agreement with the findings by Cao et al. (2016).

In our view, the model may provide a theoretical framework for analysing when a two-dose vaccination strategy is more effective than a one-dose strategy, and which is the optimal interval between doses. Clearly, a realistic model needs to include many more compartments and complex interactions. However, we believe that the idea of summarising the infection process in terms of a discrete map, and studying the properties of the discrete map is an effective method to discuss the issue.

Note that the models analysed here, like the model by Zarnitsyna et al. (2016), ignore antibody response. Definitely, the lack of antibody response is the main reason for the faster decay of infected cells than free virions when the adaptive immune response sets in (see the left panel of Fig. 3). From the biological point of view, the lack of antibody response in reinfections could be justified by focusing on heterosubtypic reinfections that differ substantially in virus proteins targeted by antibodies. Mainly, however, we believe that the models considered here are sufficiently complex and parameter rich; we believe that adding another layer of complexity would only obscure the theoretical conclusions. However, it could be quite interesting adapting this approach to models including antibody response.

As discussed in the Introduction, simple models of immune-pathogen interactions (André and Gandon, 2006; de Graaf et al., 2014; Diekmann et al., 2018; Nowak and May, 2000) yield a function F that is decreasing over most of the realistic range (i.e. the lower is immune level before the infection, the higher it will be afterwards). The analysis of different submodels of (1) allowed us to elucidate the main mechanisms behind the shape of the function F. In particular, it has emerged that model (11) in which depletion of target cells is neglected produces a function F that is initially decreasing, and is qualitatively similar to the one used by de Graaf et al. (2014). Hence, we believe that modelling the depletion of target cells (whether by viral infection, or by them turning to a refractory state) is very important in modulating the build-up of memory cells, and so the response of the immune system. We remark that depletion of susceptible target cells is an important component of the model fitted to data of experimental infection by Hadjichrysanthou et al. (2016). However, Moore et al. (2020) have recently examined, through the use of a mathematical model, data from mice infected with influenza, concluding that target cell depletion is unlikely to be an important factor in controlling influenza infections.

Heffernan and Keeling (2008) have analysed an immune-pathogen model similar to (1) and have obtained a function F (their Fig. 8) somewhat similar in shape to the one in Fig. 8. That model includes depletion of target cells; thus, one may wonder why the function F is not increasing. According to us, the reason lies in the large value of the recruitment parameter, λ_x of target cells, so that target cells recover their equilibrium density on the same time-scale as the infection, and their density decreases of a few percent at most. From this comparison, one concludes that target cell depletion must be substantial for the function F to be increasing.

A final remark concerns the simplified systems. From the comparisons of Sections 4, it has emerged that system (12) yields a qualitative behaviour roughly consistent with that obtained from more realistic models, such as (1). This means that the distinction between T-cells in the lymphoid system and in the respiratory tract, introduced by Zarnitsyna et al. (2016), does not seem to be crucial for determining the qualitative patterns of reinfections, although it definitely affects the speed of adaptive immune response. As system (12) is much simpler than (1), one might be tempted to build complex immuno-epidemiological models that include (12) as a low-dimensional ingredient. We plan to explore this possibility in future work.

References

André, J.-B. and Gandon, S. (2006), Vaccination, within-host dynamics, and virulence evolution, *Evolution (N. Y).* **60**, 13–23.

Barbarossa, M. V. and Röst, G. (2015), Immuno-epidemiology of a population structured by immune status: a mathematical study of waning immunity and immune system boosting, *J. Math. Biol.* **71**(6-7), 1737–1770.

Cao, P., Wang, Z., Yan, A. W., McVernon, J., Xu, J., Heffernan, M., Kedzierska, K. and McCaw, J. M. (2016), On the role of CD8+ T cells in determining recovery time from influenza virus infection, *Front. Immunol.* **7**(December), 611.

Cao, P., Yan, A. W. C., Heffernan, J. M., Petrie, S., Moss, R. G., Carolan, L. A., Guarnaccia, T. A., Kelso, A., Barr, I. G., McVernon, J., Laurie, K. L. and McCaw, J. M. (2015), Innate Immunity and the Inter-exposure Interval Determine the Dynamics of Secondary Influenza Virus Infection and Explain Observed Viral Hierarchies, *PLoS Comput. Biol.* **11**(8), 1–28.

de Graaf, W. F., Kretzschmar, M. E. E., Teunis, P. F. M. and Diekmann, O. (2014), A two-phase within-host model for immune response and its application to serological profiles of pertussis., *Epidemics* **9**, 1–7.

Diekmann, O., de Graaf, W. F., Kretzschmar, M. E. E. and Teunis, P. F. M. (2018), Waning and boosting : on the dynamics of immune status, *J. Math. Biol.* **77**(6-7), 2023–2048.

Dobrovolny, H. M., Reddy, M. B., Kamal, M. A., Rayner, C. R. and Beauchemin, C. A. A. (2013), Assessing Mathematical Models of Influ-

543 enza Infections Using Features of the Immune Response, *PLOS ONE*
544 **8**(2), e57088.
545 Gandolfi, A., Pugliese, A. and Sinisgalli, C. (2015), Epidemic dynamics and
546 host immune response: a nested approach, *J. Math. Biol.* **70**(3), 399–435.
547 Gilchrist, M. A. and Sasaki, A. (2002), Modeling host-parasite coevolution, *J.*
548 *theor. Biol.* **218**, 289–308.
549 Hadjichrysanthou, C., Cauët, E., Lawrence, E., Vegvari, C., De Wolf, F. and
550 Anderson, R. M. (2016), Understanding the within-host dynamics of influ-
551 enza A virus: From theory to clinical implications, *Journal of the Royal*
552 *Society Interface* **13**(119).
553 Hancioglu, B., Swigon, D. and Clermont, G. (2007), A dynamical model of hu-
554 man immune response to influenza A virus infection, *Journal of Theoretical*
555 *Biology* **246**(1), 70–86.
556 Heffernan, J. M. and Keeling, M. J. (2008), An in-host model of acute infection:
557 Measles as a case study, *Theoretical Population Biology* **73**(1), 134–147.
558 Iwasaki, T. and Nozima, T. (1977), Defense mechanisms against primary in-
559 fluenza virus infection in mice. I. The roles of interferon and neutralizing
560 antibodies and thymus dependence of interferon and antibody production.,
561 *J Immunol.* **118**(1), 256–263.
562 Li, K., McCaw, J. M. and Cao, P. (2021), Modelling within-host macro-
563 phage dynamics in influenza virus infection, *Journal of Theoretical Biology*
564 **508**, 110492.
565 Li, Y. and Handel, A. (2014), Modeling inoculum dose dependent patterns of
566 acute virus infections, *Journal of Theoretical Biology* **347**(1), 63–73.
567 Moore, J. R., Ahmed, H., Manicassamy, B., Garcia-Sastre, A., Handel, A. and
568 Antia, R. (2020), Varying Inoculum Dose to Assess the Roles of the Immune
569 Response and Target Cell Depletion by the Pathogen in Control of Acute
570 Viral Infections, *Bulletin of Mathematical Biology* **82**(3), 1–14.
571 Moore, J. R., Ahmed, H., McGuire, D., Akondy, R., Ahmed, R. and Antia,
572 R. (2019), Dependence of CD8 T Cell Response upon Antigen Load During
573 Primary Infection, *Bulletin of Mathematical Biology* **81**(7), 2553–2568.
574 Nowak, M. A. and May, R. M. (2000), *Virus dynamics: Mathematical prin-*
575 *ciples of immunology and virology*, Oxford Univ. Press.
576 Pugliese, A. and Gandolfi, A. (2008), A simple model of pathogen-immune
577 dynamics including specific and non-specific immunity, *Math. Biosci.* **214**(1-
578 2), 73–80.
579 Wu, X., Wu, P., Shen, Y., Jiang, X. and Xu, F. (2018), CD8+ Resident
580 Memory T Cells and Viral Infection, *Frontiers in Immunology* **9**, 2093.
581 Yan, A. W. C., Cao, P., Heffernan, J. M., McVernon, J., Quinn, K. M., La
582 Gruta, N. L., Laurie, K. L. and McCaw, J. M. (2016), Modelling cross-
583 reactivity and memory in the cellular adaptive immune response to influ-
584 enza infection in the host, *Journal of Theoretical Biology* **413**(November
585 2016), 34–49.
586 Yan, A. W. C., Zaloumis, S. G., Simpson, J. A. and McCaw, J. M. (2019), Se-
587 quential infection experiments for quantifying innate and adaptive immunity
588 during influenza infection, *PLOS Computational Biology* **15**(1), e1006568.

589 Zarnitsyna, V. I., Handel, A., McMaster, S. R., Hayward, S. L., Kohlmeier,
590 J. E. and Antia, R. (2016), Mathematical model reveals the role of memory
591 CD8 T cell populations in recall responses to influenza, *Frontiers in Im-*
592 *munology* **7**(MAY), 1–9.